Limitations of the thermodynamic Gibbs-Thompson analysis of nanoisland decay

Z. Kuntová,[1] Z. Chvoj,[1] V. Šíma,[2] and M. C. Tringides[3,*]
[1]*Institute of Physics, Academy of Sciences of the Czech Republic, Na Slovance 2, 182 21 Prague 8, Czech Republic*
[2]*Department of Metal Physics, Charles University in Prague, Ke Karlovu 5, 121 16 Prague 2, Czech Republic*
[3]*Department of Physics, Iowa State University, Ames, Iowa 50011, USA*
(Received 31 August 2004; revised manuscript received 16 November 2004; published 21 March 2005)

The interpretation of island-within-island decay experiments is commonly based on a quasiequilibrium analysis with the island evaporation rate related to the inverse of its curvature, i.e., the Gibbs-Thompson chemical potential $\mu(r)$, where r is the island size. However, it has been suggested that the quasiequilibrium analysis fails for sufficiently small island sizes because the distribution of atoms, with different coordination and detachment barriers at the island perimeter controls the evolution. With realistic Monte Carlo simulations that use calculated barriers for Ag(111), published in the literature and consistent with measured equilibrium island shapes, we have examined the island decay law. Deviations of the decay law of an adatom island from the expected quasiequilibrium analysis for the case of diffusion-limited kinetics are observed $N(t)=(N_0-ct)^{\alpha}$ with $\alpha\approx 1$ (instead of the expected $\alpha\approx 2/3$). In addition, the decay of a corresponding vacancy island for the same island-within-island geometry (without a step edge barrier), which is expected to be the same as the adatom island decay (in the quasiequilibrium analysis) is found to be faster. This also signals independently the failure of the quasiequilibrium analysis.

DOI: 10.1103/PhysRevB.71.125415 PACS number(s): 68.35.Fx

I. INTRODUCTION

The time evolution of nanostructures can reveal information about microscopic mechanisms and energetic barriers that control nanostructure stability.[1] As the nanostructures become smaller in size, the discreteness in their structure implies a large variation in their shape, with different types of atoms at the boundary, which in turn changes the effective controlling barrier. The ratio of the number of atoms with lower coordination (which are the ones easier to detach) to the ones with higher coordination increases as the structure size decreases. The measured macroscopic time of the island decay can be used as a probe to identify the controlling microscopic detachment barriers and changes in the barrier distribution with reduced nanostructure size.

Many important processes, which involve collective changes of the nanostructure (i.e., nanostructure coarsening, nanostructure decay, etc.) are built from individual atomistic events, i.e., the detachment of single atoms. For example, in sintering processes an initial size distribution of catalytic particles coarsens in time to larger sizes, which degrades the particle catalytic function.[2] It is still not clear how the single-atom detachment, determines the overall time in sintering. Since the catalytic particle size distribution changes, it is important to know the dependence of the detachment rate on size.

The need to know the connection between single-atom detachment rate and the evolution time of the composite structure is also evident in the diffusion of adatom or vacancy clusters.[3] Although the cluster diffuses as a collective entity with a well-defined diffusion coefficient D and the dependence D vs N (the cluster size) obeys simple scaling, it is essential to understand the origin of these universal results in terms of single-atom events, which is related to the previous question, i.e., how the single-atom detachment rate depends on cluster size.

One expects that for nanostructure sizes above some minimum, a thermodynamic description of the evolution[4] by means of an average detachment rate (in terms of a uniform chemical potential across the perimeter) is applicable. However, as the nanostructure decreases in size the atoms at the few sites of lower coordination become a larger fraction of the barrier distribution and have a larger proportionate contribution to the evolution. The presence of different types of binding sites (i.e., corner atoms, straight step atoms, kink atoms, etc.) and the larger role of fluctuations for smaller systems imply that it is not possible to use a single curvature-dependent value for the chemical potential to describe the adatom energy cost along the nanostructure perimeter. It is the purpose of this paper to study with realistic Monte Carlo simulations the failure of the thermodynamic analysis for the decay of sufficiently small island sizes. These results have general implication as to whether the physics applicable on the mesoscopic scale can be safely extrapolated to the nanoscale and more specifically are relevant to island-within-island scanning tunneling microscopy (STM) experiments monitoring the decay of a small island (adatom or vacancy) versus time located at the center of a larger vacancy island.[5]

II. THERMODYNAMIC QUASIEQUILIBRIUM ANALYSIS OF CLUSTER EVOLUTION

A standard analysis of the island evolution is based on classical theory which was developed earlier for mesoscopic size islands.[4] This approach assumes that steady state holds between atom detachment versus atom diffusion from the island. In such a description the energy cost of an atom attached to an island of radius r is given by the Gibbs-Thompson chemical potential $\mu(r)-\mu(\infty)=2\gamma/nr$ [where γ is the surface tension, $\mu(r)$ the chemical potential of an island of radius r, $\mu(\infty)$ the chemical potential of a straight

step, and n the atomic density of the island]. Atoms detach from the island faster with decreasing island size since $\mu(r)$ increases as $1/r$. In the quasiequilibrium description the balance between atom detachment and atom diffusion establishes a monomer concentration $\rho(r)$ outside the island, different from the equilibrium monomer concentration $\rho_{eq}(r)$. This difference in concentration $[\rho(r)-\rho_{eq}(r)]$ is the driving force for the island to either grow or shrink depending on its size. Since a larger driving force is present for smaller size islands the net effect is the growth of larger islands at the expense of smaller ones.

This approach was developed when the available imaging techniques lacked atomic resolution (and it was only possible to observe sufficiently large islands so a coarse-grained average was implicitly performed, which justifies the application of the Gibbs-Thompson analysis). With recently developed atom-resolving techniques (STM), it is possible to observe nanoscale size islands consisting of a small number of atoms. A natural question is under what conditions does the quasiequilibrium description in terms of $\mu(r)$ fail and is a new type of analysis necessary?

Evidence suggesting that the thermodynamic analysis fails for small clusters has been already presented for sintering processes[2] and cluster diffusion simulations.[3] In the first case it was shown with microcalorimetry that the heat of adsorption of Pb three-dimensional (3D) clusters adsorbed on MgO is smaller than the one expected from the thermodynamic relation $\mu(r)-\mu(\infty)=2\gamma/nr$ (i.e., the clusters are less stable than expected). Using the Pb bulk value for $\gamma=0.36$ eV/nm^2 the difference in measured and expected values of the energy can be as high as 0.7 eV for clusters less than 2 nm in radius. Calculation of the adsorption energy by taking into account the binding of the lower coordination atoms at the perimeter (i.e., not assuming an idealized spherical shape) was used to deduce a value of the adsorption energy closer to the experimental one. Using these lower values of the adsorption energy as a function of size, better agreement was found between the observed and predicted change in the cluster size distribution, after annealing an initial cluster distribution generated at lower temperature.

Deviations from the thermodynamic description of island shapes were also noted in the equilibrium studies of Ag island shapes grown epitaxially on Ag(111).[6] The shape of these islands was determined with STM as a function of temperature to contain two kinds of segments: straight and kinked. The ratio of the two types of segments was measured and compared to a simple thermodynamic analysis based on the free energy for the two types of segments expected from Ising model. Deviations from this model (and the need to treat the exact shape of the island perimeter with realistic simulations) were noted for islands containing less than 5000 atoms, which is four times the island size of interest in the present study and in the island decay Ag(111) experiments.[5]

Similarly, simulations[3] to deduce the adatom and vacancy cluster diffusion coefficients D [relevant to Xe/Pt(111) experiments] have shown that the dependence of D on cluster size N is not consistent with the N^{-1} expected for periphery diffusion prediction and the quasiequilibrium analysis; instead the diffusion coefficient D is determined only by the most "active" atoms, i.e., the ones with two nearest neighbors that have the lowest detachment barrier. A simple nearest-neighbor attractive interaction ε was assumed in the model with the detachment barrier given by the initial energy at a given site, i.e., the number of nearest-neighbor (NN) bonds z times the NN enegy $z\varepsilon$. Depending on how the number of these most "active" atoms varies with cluster size, different scaling forms for D are obeyed (i.e., it was found that the number of the most "active" atoms scales as $N^{-1/3}$ for the adatom and $N^{-3/4}$ for a vacancy clusters). More importantly the diffusion activation energy for vacancy cluster is higher than the one for an adatom cluster (i.e., by approximately 15%), as a result of the essential asymmetry between adatom and vacancy cluster shape (i.e., convex for adatom versus concave for vacancy cluster). This asymmetry will be discussed below in the context of adatom versus vacancy island decay experiments.

Deviations from the thermodynamic analysis were also found in the coarsening of homoepitaxial islands grown on Ag(100).[7] The coalesescence of two separate islands of size L meeting at a corner to form a single island was monitored in time for different island sizes. The key microscopic process operating is the diffusion of atoms along the island perimeter. Both STM experiments and Monte Carlo simulations show deviations from the expected thermodynamic dependence of the time t for the process to be completed (i.e., the time scales like L^3 instead of L^4). This deviation was accounted for by a kink rounding barrier, which becomes the rate limiting step at sufficiently low temperature or small L (and not the diffusion process along the perimeter L). The simulations in Ref. 7 were also based on nearest-neighbor bond counting with a term $z\varepsilon$ added to the total barrier encountered by the diffusing atom. In both Refs. 3 and 7 the hopping algorithm involves only the initial energy of the diffusing atom. Since the algorithm in the current study is different and the breakdown of the thermodynamic analysis depends on the algorithm applied, the physical significance of the chosen algorithm will be discussed below.

III. ADATOM AND VACANCY ISLAND DECAY EXPERIMENTS

These considerations apply to STM experiments (mostly on homoepitaxial metal systems) in a widely used island-within-island geometry to deduce microscopic barriers, i.e., the detachment barrier, the line tension, the step edge barrier, etc. The experiments are based on the comparison between the decay rates of small adatom versus vacancy islands of radius r located in the center of larger vacancy islands of radius R. It has been observed that the small vacancy island decays over a longer time than the decay of the adatom island (by approximately a factor of 25 at 300 K).[5]

In the standard analysis[4] of island decay it is assumed that the steady state holds, i.e., the number of atoms detached is balanced by the diffusion current away from the island. The detachment rate depends on island size according to the Gibbs-Thompson dependence. The decay rate of the adatom island involves two processes, i.e., atoms released by the island to the terrace that eventually attach at R (a positive

term) and atoms emitted by the island at R that diffuse back and are adsorbed at the small island (a negative term),

$$\frac{dA_a}{dt} = -[(2\pi ra)P_r E(r) - (2\pi Ra)P_R E(-R)], \qquad (1)$$

where $A_a = N_a/n$ is area of the adatom island (N_a the number of sites and n the 2D density of the island), $E(r)$ and $E(-R)$ are the detachment rates defined as the inverse of the times τ_a and τ_v for all perimeter atoms to detach $E(r) = 1/\tau_a$ and $E(-R) = 1/\tau_v$ for the adatom island and the larger vacancy island, respectively, P_r is the fraction of the detached atoms from r that attach at R (i.e., $1 - P_r$ is the fraction returning back to r), and P_R is the fraction of atoms detached at R and attached at r. Since $E(r)$ and $E(-R)$ are averaged over the island perimeter, they need to be multiplied by $2\pi ra$ with a the lattice constant.

In the quasiequilibrium approach the atom detachment rate[4] $E(r)$ is related to the terrace diffusion D_t and ρ_{eq}, the equilibrium concentration in front of the island via the steady state condition $\rho_{eq}(r) = E(r)/D_t$. The equilibrium concentration in front of an island of radius r is determined from its curvature $\rho_{eq}(r) = \rho_\infty \exp[\gamma/kTnr]$, where ρ_∞ is the equilibrium concentration in front of a straight step and γ the 1D "surface" tension. Using these relations, Eq. (1) leads to

$$\frac{dA_a}{dt} = -D_t\rho_\infty\left[(2\pi ra)P_r \exp\left(\frac{\gamma}{kTnr}\right) - (2\pi Ra)P_R \exp\left(-\frac{\gamma}{kTnR}\right)\right]. \qquad (2)$$

The expressions for the probabilities P_r and P_R are $P_r \cong a/r \ln(R/r)$ and $P_R \cong a/R \ln(R/r)$.[8] If we approximate $\exp(-\gamma/kTnR) \approx 1$ because $R \gg r$ and linearize the other terms $\exp(\gamma/kTnr) \approx 1 + (\gamma/kTnr)$ and $\exp(-\gamma/kTnr) \approx 1 - (\gamma/kTnr)$, respectively, we have

$$\frac{dA_a}{dt} = -D_t\rho_\infty \frac{2\pi a^2}{\ln(R/r)}\frac{\gamma}{kTnr} \approx -\frac{c_1}{r} \qquad (3)$$

with $c_1 = D_t\rho_\infty(2\pi a^2)\gamma/kTn$.

Since r is proportional to $A_a^{1/2}$ the integration of the above equation leads to a time-dependent decay law $A_a = (A_0 - c_1 t)^{2/3}$. This is how the experiment was analyzed in Ref. 5 to extract the step edge barrier $\Delta E_s = 0.13$ eV, prefactor ratio $\nu_s/\nu_t \sim 1$, and 1D "surface" tension $\gamma = 0.22$ eV/atom [which justifies the linearization of the exponential $\exp(\gamma/kTnr)$ since $\gamma/kTnr = 0.1$ for Ref. 5. One additional implication of the steady state assumption is that the ratio of the detachment rates $E(r)/E(-R)$ of the adatom versus vacancy islands is slightly larger than 1 [i.e., using the extracted parameters for Ag/Ag(111) under the condition of quasiequilibrium, this ratio is $\exp[\gamma/(kTn)(1/r + 1/R)] \approx 1.57$ for $r = 7$ nm and $R = 70$ nm (Ref. 5)].

The quasiequilibrium description assumes a circular island shape and that all perimeter atoms are equivalent. However, the shape of the island is not circular, but it shows 1D facets because free energy minima exist in preferred high-symmetry orientations. For well-equilibrated islands in contact with a "sea" of monomers on the terrace, the shapes were determined with STM.[6] Because of the threefold symmetry of the fcc(111) crystal the shape is hexagonal with six straight segments separated by kinked segments. At the temperatures of interest $T \sim 300$ K, the ratio between straight and kinked segment is approximately 1.

An alternative way was proposed to analyze island decay experiments in terms of an independent detachment model,[9] which takes into account the experimentally determined island shapes. This model does not assume that the island is at equilibrium with the monomers, but the detachment rate of an atom with a given coordination simply depends on the corresponding local barrier $z\varepsilon$, i.e., the number of nearest-neighbor bonds times the NN energy. Atoms at the kinked segments that have lower coordination of three nearest-neighbor bonds evaporate first while atoms at the straight segments that have four bonds evaporate slower. If the goal is to determine the island shape at equilibrium, it is possible to reformulate the difference in the local barriers at the perimeter in terms of a position-dependent chemical potential as carried out for the relaxation of a "groove" in Ref. 10. But as stated in Ref. 10 such a description will not be applicable on the nanoscale, when the atomic structure of the decay groove should be taken into account, which is the primary objective of the current study.

There is a basic asymmetry between atom evaporation from straight segments for adatom versus vacancy islands already noted in Ref. 3. Since straight segments on adatom islands have end atoms that have three nearest neighbors [i.e., kinked atoms and corner atoms have the same coordination on fcc(111) surfaces], the atoms can detach sequentially as the straight segment "unzips" from its corners. This process is faster than the detachment of atoms from straight segments on vacancy islands, since the islands are concave and corner atoms have five nearest neighbors so they cannot initiate the unzipping. It is necessary for an atom on a straight segment to evaporate but this requires a longer time than the evaporation of a corner atom by approximately a factor of $\exp(\varepsilon/kT)$ (since it involves the breaking of one more bond).

We can now write expressions for the adatom island decay within the independent detachment model:

$$\frac{dA_a}{dt} = -[(2\pi ra)E(r)P_r - (2\pi Ra)E(-R)P_R] \approx -(2\pi ra)E(r)P_r = -(2\pi ra)(1/\tau_a)P_r = -c_2 \qquad (4)$$

with $c_2 = -(2\pi a)(1/\tau_a)[a/\ln(R/r)]$, essentially a constant, since $rE(r)P_r \gg RE(-R)P_R$, the second term, is neglected. This gives a decay growth law different from the one deduced from the quasiequilibrium analysis $A_a = A_0 - c_2 t$. Similar expressions are derived for the vacancy island decay with P_{Rs} the probability for an atom detached from R to attach at r after overcoming the barrier with interlayer probability $s = \nu_s/\nu_t \exp(-\Delta E_s/kT)$ with ΔE_s the step edge barrier:

$$\frac{dA_v}{dt} = (2\pi aR)E(-R)P_{Rs}.$$

The functional relation between P_{Rs} and r depends on the strength of s. For strong barriers $s \ll P_r$ P_{Rs} simplifies

to sr/R, and leads to a proportionality between the decay rate dA_v/dt and r [which implies a decrease in time as $A_v=(A_0-c_3t)^2$ with $c_3=(4\pi as)/\tau_v$]. On the other hand, for a weak barrier $s \gg P_r$ the barrier is irrelevant and $P_{Rs} \approx P_R$, which leads to a linear decay growth law $A_v=A_0-c_4t$, with $c_4=(2\pi a^2)/[\tau_v \ln(R/r)]$.

The main conclusion from this analysis is that depending on the details of the microscopic mechanism controlling island decay, different time-dependent laws are possible. Another experimental parameter that can be used to differentiate between different models (which is easily measurable) is the ratio of the average adatom to vacancy island decay rates. For the detachment model this is given by

$$\frac{E(r)}{E(-R)} = \frac{r}{R}\frac{\tau_v}{\tau_a}$$

and can be larger than 1 since it depends on the two times τ_v, τ_a, which can be very different depending on the nearest-neighbor bond energy ε and for hopping algorithms that depend on the initial site energy.[3,7,9] On the other hand, for the quasiequilibrium analysis this number is closer to 1 as noted above.[5]

It is interesting to point out other differences between the two ways of analysis. In the quasiequilibrium analysis it is not possible to separate out the two contributions, i.e., the line tension γ and the detachment rate $E(r)$ since they enter in a combined way to the decay rate dA_a/dt, while in the independent detachment model only $E(r)$, but not γ, is the relevant quantity.

Earlier simulations with the island-within-island geometry were carried out in an Ising-like model to test the condition of applicability of the quasiequilibrium analysis.[11] Although the goal of the study is similar to the work described here and most of the conclusions reached are consistent, there are also differences. The study in Ref. 11 was carried out on a square lattice with an initial circular shape, so there were no clear 1D facets of straight and kinked segments as for the triangular lattice. The temperature of the simulation was higher than the one used in the current simulation or, more importantly, since different barriers E_{if} from initial site i to final site f were used, the ratios of E_{if}/kT were on average 2.5 times larger in the current simulation than in Ref. 11. The algorithm was based both on initial and final site energies with the barrier for detachment from straight step sites ($z=3$) versus detachment from corner sites ($z=2$) slightly increased. Conditions for the power law validity of the island decay $A(t)$ (which for the diffusion-limited case implies that the decay exponent is $\alpha=2/3$) are as follows: first, the line tension γ is sufficiently small [so the expansion in Eq. (2) is justified], and second, a larger difference $R \gg r$ between the radii of the large vacancy island R and the small island at its center [so the monomer density $\rho(r)$ can reach equilibrium]. The sizes used in the simulation of Ref. 11 were $r=15$ and $R=40$, slightly worse for the quasiequilibrium analysis condition to hold (than the sizes in the current simulation $r=20$ and $R=70$), but the expansion in Eq. (2) is better justified in Ref. 11. Two cases were used, corresponding to very low terrace and very high terrace diffusion. Despite the higher temperature and lower E_{if}/kT (and therefore the reduced importance of different types of sites at the island perimeter) deviations from the expected exponent $\alpha=2/3$ were observed, indicating failure of the quasiequilibrium analysis. However, the main test in the study was to check whether the full decay curve can be obtained from the numerical solution of Eq. (2) with the controlled phenomenological parameters D (the terrace diffusion) and detachment rates $E(r)$ and $E(-R)$ measured independently in separate simulations of different quantities, i.e., the frequency of hopping on the terrace and the time constant of the autocorrelation of the interface fluctuations respectively.

IV. MONTE CARLO SIMULATIONS OF THE ISLAND DECAY PROCESS

Since different methods lead to different decay laws, we have performed Monte Carlo simulations to monitor the decay both of the adatom and the vacancy island to test whether the assumptions in each method are justified. These simulations are more realistic than other models since all the microscopic barriers are based on independent information in the literature and without any preconditions imposed. Additional input to the simulations is the initial island shape. The initial shape was the one determined by the equilibrium island shape at 300 K,[6] i.e., a hexagonal island with straight and kinked segments of equal number of atoms. No assumption was made that the barriers should follow simple bond counting, as assumed in the independent detachment model. The barriers were based on the calculated ones by two different groups for Ag(111),[12,13] since the ultimate goal in the future is to understand the energetics of Ag(111). This paper discusses the applicability of the Gibbs-Thompson analysis while future work will concentrate on the prefactor question for Ag/Ag(111). For the diffusion prefactors we made the common assumption[1] that all the different processes have the same prefactor. This should not affect the main conclusion of the current study concerning the island decay mechanism at the low temperature 300 K, since the variation of the hopping probabilities due to differences in the local barriers is larger than prefactor variations by 2–3 orders of magnitude.

The first column of Table I lists the type of microscopic processes and the next two columns denote the literature barriers from Refs. 12 and 13. The last column lists the barriers used in this study. The microscopic processes are described by the number of neighbors in the initial (n_i) and the final (n_f) position. Since the two Refs. 12 and 13 do not include all the required barriers we have extended the table by adding the missing barriers so the island shape observed in the simulation is consistent with the shape from Ref. 6.

Figure 1 shows visually the microscopic processes of Table I with both the initial and final state of the hopping atom indicated. In addition from Ref. 6, it is found that essentially there is no difference between the formation energies of A- and B-type steps and both types of steps occur with the same probability. This implies that all the microscopic barriers for the A-and B-steps for Ag/Ag(111) are the same, although the calculations show differences between the two types of barriers.[12,13]

TABLE I. A list of the microscopic barriers calculated theoretically for Ag(111) and available in the literature, column 2 from Ref. 12, column 3 from Ref. 13, and column 4, the adjusted barriers used in the simulation. The adjustment was based on the experimentally determined island shapes from Ref. 6 and the absence of anisotropy between A- and B-type steps.

Type of process	Ref. 12		Ref. 13		Used in MC
	step A	step B	step A	step B	
$0\rightarrow 0$	0.061		0.067		0.061
$1\rightarrow 0$	—	—	0.315		0.315
$1\rightarrow 1$	—	—	0.077	0.132	0.077
$1\rightarrow n_f>1$	—	—			0.290
$2\rightarrow 0$	0.758	0.691	—	—	0.520
$2\rightarrow 1$	—	—	0.257	0.317	0.317
$2\rightarrow 2$	0.294	0.338	0.221	0.296	0.300
$2\rightarrow n_f>2$	—	—			0.290
$3\rightarrow 0$	—	—	—	—	0.650
$3\rightarrow 1$	—	—	0.423	0.478	0.478
$3\rightarrow 2KR$	0.579	0.582	—	—	0.582
$3\rightarrow 2$	0.471	0.540			0.540
$3\rightarrow 3$	—	—	0.387	0.457	0.382
$3\rightarrow n_f>3$	—	—			0.290
$4\rightarrow 1$	0.571	0.527	—	—	0.780
$4\rightarrow 2$	—	—	—	—	0.580
$4\rightarrow 3$	—	—	—	—	0.400
$4\rightarrow 4$	—	—	—	—	0.550
$4\rightarrow n_f>4$	—	—	—	—	0.290
Descent down	0.130		0.240		variable

The algorithm used does not depend only on the initial site energy defined by the number of nearest-neighbor bonds as in Refs. 3, 7, and 9. In the initial site energy algorithms there are only five different hopping configurations to be considered, since the final site the atom is jumping into is irrelevant, while for the algorithm used in this work, both the initial and final configurations are relevant. In principle there are 2^8 independent processes, but since this number is so high the same rate was assigned to processes with the same number of initial and final nearest neighbors (as in Ref. 11). With this algorithm the two detachment rates $E(r)$ and $E(-R)$ become closer (for $r=20$ and $R=70$, the ratio is 1.6 for the set of interactions used here) but with the initial energy algorithm the ratio is much larger than 1. As argued in Ref. 9 and also observed in Ref. 3 the asymmetry between the shapes of the adatom (convex) versus vacancy island (concave) requires the detachment of atoms from straight segments in the case of the vacancy island, which is slower by a factor of $\exp(\varepsilon/kT)$. Part of the reason for the reduced ratio is the similarity of the barriers from kinked $(3\rightarrow 0)$ and from straight segments $(4\rightarrow 1)$ than the barriers of the algorithm in Refs. 3, 7, and 9. In addition, with the algorithm used here, there are many intervening processes that can transfer material across the island perimeter (i.e., fast edge diffusion, smaller barriers for $4\rightarrow 2$, $4\rightarrow 3$, etc.) such that once a fluctuation generates one of these configurations that has lower barrier, they act as intermediate processes. These processes lead to the eventual detachment of the atom, thus allowing atoms from straight segments to be released more easily and bringing the two detachment rates $E(r)$ and $E(-R)$ closer.

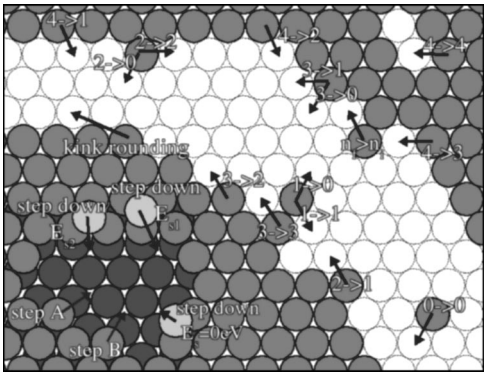

FIG. 1. Schematic illustration of the different microscopic processes used in the simulation with the number of initial and final nearest neighbors also indicated. The barriers shown in Table I are based on the calculated ones for Ag(111) available in the literature.

Inspecting Table I we can summarize the physical significance of the chosen barriers and how they are related to experimental results about Ag/Ag(111):

(i) Terrace diffusion on Ag/Ag(111) is very fast,[14] with a ratio between the average detachment time to the terrace hopping time of a single Ag atom 10^9 at 300 K, which is reflected in the very low terrace diffusion barrier 0.061 eV.

(ii) The detachment from a kinked segment (where the atom has three neighbors) is easier than the detachment from a straight segment (where the atom has four nearest neighbors) although this difference is smaller than the expected one from simple bond counting with an algorithm based on the initial site energy. Within the current algorithm, the detachment is not direct but through a two-step process. Detachment from a kinked segment first involves the process $3\rightarrow 1$ (with barrier 0.650 eV) followed by the process $1\rightarrow 0$ (with barrier 0.315 eV) and detachment from a straight segment first involves the process $4\rightarrow 1$ (with barrier 0.780 eV) followed by the process $1\rightarrow 0$ (with barrier 0.315 eV). The difference between detachment from a kinked segment and from a straight segment is effectively only 0.13 eV while with the bond counting algorithm it would be $\varepsilon=0.22$ eV.[9]

(iii) Edge diffusion $1\rightarrow n_f$ (0.290 eV) and $2\rightarrow 2$ (0.3 eV) is very fast compared with the average detachment since its barrier is less than half the lowest detachment barrier.

The island shape is sensitive to the chosen barriers since the higher effective barrier determines the slowest process and the most stable orientation. For example, if the detachment barriers for A- and B-type steps are different, then anisotropic island shapes are observed with the step of the lowest detachment barrier being the one with the shortest segment. The barriers are more complex than the simple bond counting barriers, but more realistic, since they are determined from the optimal diffusion pathway and substrate relaxation is included.

For the simulations initially a small adatom or vacancy island of radius 20 lattice constants is positioned at the center of the larger vacancy island of radius 70 lattice constants. This larger vacancy island is smaller than the one in the experiment (~200 lattice constants) to speed up the program, since it only affects the geometric parameters, i.e., capture probabilities P_r and P_R but not the energetics and the detachment rates. Both islands initially have hexagonal symmetry with straight and kinked segments of equal length alternating at the perimeter as found experimentally.[6] The initial concentration in the region between the adatom and vacancy islands is zero as in the island experiment.[5]

Since the barriers in the simulation differ by a factor of two, which implies that the corresponding rates differ by orders of magnitude, a kinetic Monte Carlo (KMC) simulation was chosen within the Bortz-Kalos-Lebowitz implementation[15] to optimize code efficiency. The KMC follows changes on the surface after each hop; the time between hops is not constant (as in classical MC) but depends on the barrier distribution. The time for the KMC step we obtain is $\Delta t = \ln(\xi)/\Sigma_{i=0}^{\text{number of class}} n_i p_i$, where ξ is a random number within (0,1), n_i is the number of atoms with the same hopping barrier i, and p_i is probability of jump per time unit of one atom from this class i. Essentially the time for a KMC step is given by the inverse of the total sum of probabilities for each atom on the surface and it is independent of the kind of movement chosen. As a time unit we use the average time for jumps on the terrace so the relative probability p_i of jump within class i can be written as $p_i = \exp[-(E_i - E_{0\to 0})/kT]$, where E_i is the diffusion barrier for class i and $E_{0\to 0}$ is the barrier terrace diffusion ($E_{0\to 0} = 0.061$ eV). As the atoms with the lowest barrier are reduced, this is manifested as an increase in the time intervals between successive hops. The temperature of the simulations was $T = 300$ K, the same as in Refs. 5 and 6, where the equilibrium Ag(111) island shapes were determined. The absolute value of the temperature is not essential as long as it is sufficiently low so the island develops different facets (i.e., straight vs kinked segments) which have drastically different detachment barriers. With increasing temperature the island shape becomes rounded and the conditions for applying the steady state analysis should be better met. With increasing temperature the breakdown of the Gibbs-Thompson analysis should occur at smaller island sizes

Figure 2 shows pictures of the island decay for different times, Fig. 2(a) for time $t = 0$ t.u., when the central adatom island has 1700 atoms, and Fig. 2(b) for time $t = 5.7 \times 10^{10}$ t.u., when the smaller adatom island has 300 atoms. The island orientation is such that a kinked segment is at the island top and the other five equivalent kinked directions are rotated by $n\pi/3$ ($n = \bar{1}, 2, 3, 4, 5$) radians while the straight segments (along the $\langle 1\bar{1}0 \rangle$ direction) are $\pi/6$ radians off these directions. The B-type segment is the straight segment to the right side of the island and the two equivalent B-type steps are rotated by $2n\pi/3$ ($n = 0, 1, 2$).

The initial island shape is seen in Fig. 2(a) with both kinked and straight segments marked. With time the island decreases and at the same time both straight and kinked segments develop considerable roughness. Although these

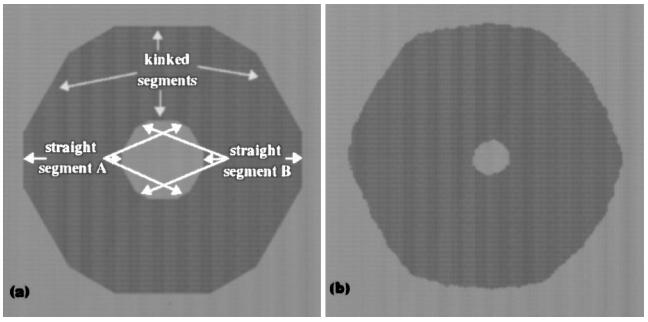

FIG. 2. (a) Snapshot of the system at $t = 0$ for an adatom island with $r = 20$ and $R = 70$. The number of atoms in the adatom island is 1700. Kinked segments (along $\langle 211 \rangle$), A-type steps along $\{[\bar{1}01], [1\bar{1}0], [01\bar{1}]\}$, and B-type steps along $\{[\bar{1}0\bar{1}], [0\bar{1}1], [10\bar{1}]\}$ are marked. (b) The adatom island evolution after $t = 5.7 \times 10^{10}$ t.u. with rounded shapes as in Ref. 6. Both the adatom island and the large vacancy island perimeter show considerable roughness. Along the large vacancy island boundary kinked segments are still visible.

changes are also visible in the small decaying island they are better recognizable at the perimeter of the large vacancy island. At its perimeter the kinked segments are more visible and better preserve their orientation, with smaller roughness than the straight segments. Part of the roughness on the straight segments is caused by well-developed nanofacets built from a small number of atoms (less than ~20) with their side 1D facets oriented along the original $\langle 1\bar{1}0 \rangle$ directions. Faster edge diffusion on a straight step (i.e., processes $1 \to n_f$) moves single atoms from the straight to the kinked segment, or promotes the nucleation of 1D islands which grow into nanofacets. These nanofacets are stable and reduce the transfer of material from the straight to the kinked segments of the large vacancy island. The dynamic balance between all the processes results in rough but rounded shapes, where atoms of lower coordination (kinked atoms) and atoms of higher coordination (straight step atoms) are still present on both the original kinked and the straight segments. On the other hand, with the initial energy bond counting algorithm the straight step segments will grow at the expense of the kinked segments.

Figure 3 shows the dependence of the number of atoms of the small adatom island as a function of time. As discussed before, the steady state predicts that the decay will follow a dependence on time with an exponent 2/3 because the decay rate dA_a/dt is inversely proportional to the island radius $1/r$. As seen in Fig. 3 the best fit to the data is $N(t) = (N_0 - ct)^{\alpha}$ with $\alpha = 1$. Only at the end, when the island size is less than ~15% its original size and the adatom island shape is irregular, a smaller exponent $\alpha \approx 3/4$ is consistent with the tail of the decay. This indicates the change of the decay mechanism.

Figure 4 shows the term $[E(r) - E(-R)]/\ln(r/R)$ versus time, which as seen in Eqs. (1) and (2) defines the dependence of the decay rate on r and can account for the linearity in the time dependence of the island size with time in Fig. 3. This term in Fig. 4 is practically constant in time instead of following an increase according to the increasing $1/r$ ex-

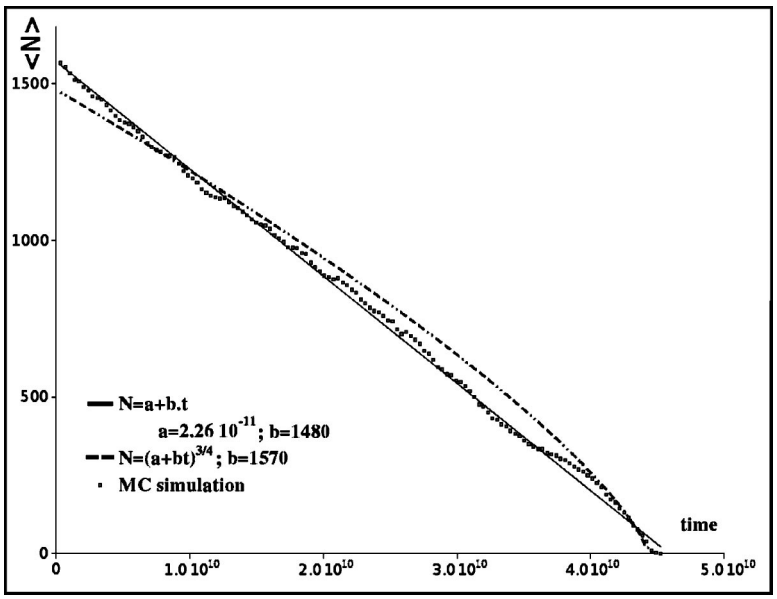

FIG. 3. N vs t, the number of atoms in the small adatom island vs time. Initially the radius is $r=20$, $R=70$ and the shape consists of straight and kinked segments of equal number of atoms. Data were fitted to $N(t)=(N_0-ct)^{\alpha}$ with $\alpha\approx 1$ different from the value expected for the "diffusion-limited" quasiequilibrium analysis $\alpha\approx 2/3$.

pected from steady state [since $E(r)\gg E(-R)$]. The island size has dropped by approximately a factor of 2.3 during this interval. One should expect an increase in the plotted parameter by the same factor. Although the data are noisy and there is a slight increase with time, this increase is much less than the expected one.

Scaling analysis has also been applied to the decay of the 2D layers, which are parts of initial metastable 3D nanostructures in different initial geometries.[16] Different decay exponents are observed that are functions of the nanostructure geometry (whether it has a cone or a paraboloid shape). However, recent simulations to describe the decay of 3D nanostrutures have shown deviations from the expected universal power laws and have been attributed to the breakdown of the quasiequilibrium analysis. A phenomenological fit to the decay was still possible if the dependence of dA/dt on A includes a second term that decreases with decreasing A.[17] Such a term can be related to the changing shape of the nanostructure and the increasing role in the decay of sites with lower coordination. The presence of both terms can lead to nonuniversal values of the decay exponents. As discussed before in Ref. 11 the time dependence of the island decay is shown for slow terrace and fast terrace diffusion. Because of the higher temperature used no facets develop at the island perimeter and no large variation in the local detachment barriers occurs, so the effects motivating this work are less pronounced. However, the decay curves shown are consistent with a decay law faster than $a=2/3$ expected for the diffusion-limited decay, especially at very long times when the island decreases to less than 10% of its original size. Even at such high temperatures when no distribution of barriers is expected at the island perimeter, deviations from its initial decay rate are observed when the island reaches sufficiently small size and develops considerable roughness.

Figure 5 shows stronger evidence against the quasiequilibrium analysis. The simulation was run with a small va-

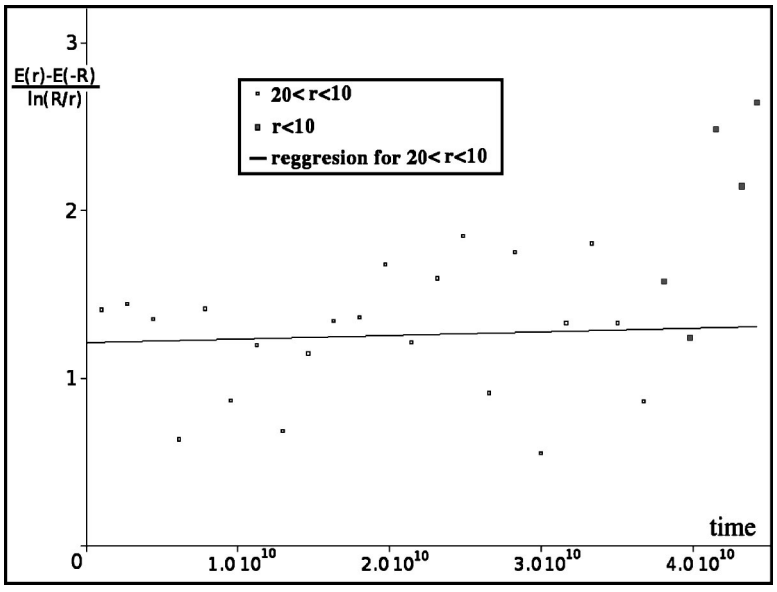

FIG. 4. $[E(r)-E(-R)]/\ln(r/R)$ vs t for the small adatom island of radius $r=20$. Although the data are noisy they do not show the expected $1/r$ dependence from the quasiequilibrium analysis. The much weaker dependence on r is consistent with the value $\alpha\approx 1$ found in Fig. 3.

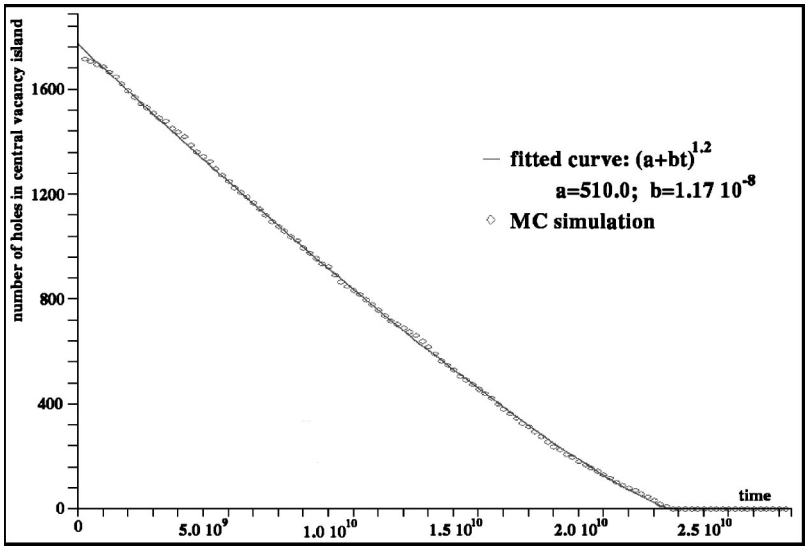

FIG. 5. N vs t for the small vacancy island (with zero step edge barrier) showing that the time of the vacancy island to evaporate is less by a factor 2.8 than the decay time of the adatom island, while the quasiequilibrium analysis predicts the times to be the same. A slightly larger exponent $\alpha \approx 1.2$ is found for the small vacancy island evaporation, indicating a decreasing rate dA/dt with decreasing r.

cancy island of the same size (as the adatom island) at the center of the large vacancy island, but zero step edge barrier at its perimeter. This barrier controls the hopping of atoms from the terrace into the small vacancy island. [Simulations that show how the refilling depends on a finite step edge barrier and how to extract the step edge barrier for Ag/Ag(111) will be presented in the future.[18]] The case of zero step edge barrier is still "diffusion limited" (according to the classification based on the steady-state analysis[4]) so one expects an identical growth law to hold (as for the adatom island decay) since in both cases one obtains exactly the same decay [Eq. (3)]. However, the results of the simulation do not confirm this as shown in Fig. 5. The decay law for the small adatom and the small vacancy island are different. The decay exponent for the small vacancy island is 1.2 (slightly larger than 1, which implies that the decay rate dA_v/dt decreases as r decreases). More surprisingly, the time needed for the small vacancy island to evaporate is shorter by a factor of 2.8 from the evaporation time of the small vacancy island. Part of the reason for this different factor is that for the case of the small vacancy island the decay rate is simply proportional to the negative term $E(-R)$ [since the $E(-r)$ term releases atoms at the small vacancy island perimeter, which are readsorbed somewhere else on its perimeter] and implies $E(-r) \approx 0$. For the small adatom island the decay rate is proportional to the difference $E(r) - E(-R)$. Because in the chosen algorithm $E(r)$ and $E(-R)$ are close, their difference is smaller in absolute value than $E(-R)$, the rate of the vacancy island.

V. CONCLUSIONS

We have presented realistic simulations of island-within-island decay processes that show that for sufficiently small structures the thermodynamic quasiequilibrium analysis fails and there is a need of an alternating approach that takes into account explicitly the distribution of energetic barriers at the island perimeter. Similar conclusions have been reached in other time-dependent processes that involve nanostructure evolution, i.e., sintering in Pb nanoclusters and nanocluster diffusion. The results of the simulation are based on a model that inputs calculated barriers for Ag(111) available in the literature and adjusts them to be consistent with experiments on equilibrium island shapes. Initially the island shape has an equal mixture of straight and kinked segments as observed experimentally. These barriers and the hopping algorithm are not equivalent with simple nearest-neighbor bond models, which take into account only the initial site energy. The results show that for the case of small adatom or vacancy islands the decay law deviates from the expected diffusion-limited exponent $\alpha = 2/3$ (and instead $\alpha \approx 1$ is found). The decay of a small adatom versus small vacancy island (without a step edge barrier) is equivalent in the quasiequilibrium analysis, but the simulation shows that vacancy decay is 3 times faster, which also confirms the limitations of the quasiequilibrium. For these reasons the quasiequilibrium analysis should be applied with care in the interpretation of the island-within-island decay experiments.

ACKNOWLEDGMENTS

Ames Laboratory is operated for the U.S. Department of Energy by Iowa State University under Contract No. W-7405-Eng-82. This work was supported by the Director for Energy Research Office of Basic Energy Sciences (MCT). Financial support for the collaboration was also provided by Grant No. NSF-INT-0308505 (USA), Grant Agency of Academy of Sciences of Grant No. IAA1010207 (CR), and MSMT Grant No. ME 655 (CR) and FRVS 1840/2004.

*Author to whom correspondence should be addressed. Electronic address: tringides@ameslab.gov

[1] *Surface Diffusion: Atomistic and Collective Processes*, edited by M. C. Tringides (Plenum, New York, 1997); "*Collective Diffusion on Surface: Correlation Effect and Adatom Interaction*" edited by M. C. Tringides, and Z. Chvoj (Kluwer, Dordrecht, 2000).

[2] C. T. Campbell, S. C. Parker, and D. E. Starr, Science **298**, 811 (2002).

[3] D. S. Sholl and R. T. Skodje, Phys. Rev. Lett. **75**, 3158 (1995).

[4] P. Wynblatt and N. A. Gjostein, Prog. Solid State Chem. **9**, 21 (1975).

[5] K. Morgenstern, G. Rosenfeld, E. Laegsgaard, F. Besenbacher, and G. Comsa, Phys. Rev. Lett. **80**, 556 (1998).

[6] M. Giesen, C. Steimer, and H. Ibach, Surf. Sci. **471**, 80 (2001); Ch. Steimer, M. Giesen, L. Verheij, and H. Ibach, Phys. Rev. B **64**, 085416 (2001).

[7] D. J. Liu, C. R. Stoldt, P. A. Thiel, and J. W. Evans, Mater. Res. Soc. Symp. Proc. **749** W2.8.1 (2003); D. J. Liu, and J. W. Evans, Phys. Rev. B **66**, 165407 (2002).

[8] G. Rosenfeld K. Morgenstern, and G. Comsa, in *Surface Diffusion: Atomistic and Collective Processes*, edited by M. C. Tringides (Plenum, New York, 1998), p. 361.

[9] Z. Chvoj and M. C. Tringides, Phys. Rev. B **66**, 035419 (2002).

[10] W. W. Mullins, J. Appl. Phys. **28**, 333 (1957).

[11] J. G. McLean, B. Krishnamachari, D. R. Peale. E. Chason, J. Sethna, and B. H. Cooper, Phys. Rev. B **55**, 1811 (1997).

[12] J. Jacobsen, B. H. Cooper, and J. P. Sethna, Phys. Rev. B **58**, 15847 (1998).

[13] Z. Chvoj, C. Ghosh, T. S. Rahman, and M. C. Tringides, J. Phys.: Condens. Matter **15**, 5223 (2003).

[14] K. Bromann, H. Brune, H. Roder, and K. Kern, Phys. Rev. Lett. **75**, 677 (1995).

[15] A. B. Bortz, M. H. Kalos, and J. L. Lebowitz, J. Comput. Phys. **17**, 10 (1975).

[16] A. Ichimiya, K. Hayashi, E. D. Williams, T. L. Einstein, M. Uwada, and K. Watanabe, Phys. Rev. Lett. **84**, 3662 (2000).

[17] F. Nita and A. Pimpinelli, Surf. Sci. **551**, 31 (2004).

[18] Z. Kuntova, Z. Chvoj, and M. C. Tringides (unpublished).